UDC 627.8:621.311.21:550.837.76
IRSTI 70.17.29
RESEARCH ARTICLE

GROUND-PENETRATING RADAR DIAGNOSTICS OF THE TECHNICAL CONDITION OF LOAD-BEARING STRUCTURES OF THE KAPCHAGAY HYDROPOWER PLANT UNDER LONG-TERM OPERATION

G.T. Kareken[1]*, Zh.N. Moldamuratov[1], N.I. Vatin[2], N.A. Shanshabayev[1,3], A.A. Bryantsev[1,4], S.Ye. Orazov[1]

[1]International Educational Corporation, 050043, Almaty, Kazakhstan
[2]Peter the Great St. Petersburg Polytechnic University (SPbPU), 195251, St. Petersburg, Russia
[3]LLP «StroyTechExpertiza», Taraz, Kazakhstan
[4]LLP «RAS Engineering Research Institute», Almaty, Kazakhstan

Abstract. *Hydraulic structures and their soil foundations degrade during long-term operation, often through hidden subsurface defects. This study used ground-penetrating radar (GPR) to assess the subsurface condition of the Sh. Chokin Kapchagay hydropower plant (Kazakhstan), in service for over 50 years in a zone of seismic intensity 8. Sixty-two records were acquired with an OKO-3 system (150 and 400 MHz antennas) on six elements: the powerhouse platform, the tailrace channel lining, the upstream slope protection of the river-bed and ravine dams, the 220 kV switchyard platform and the stop-log storage area. Wave velocities were derived from diffraction hyperbolas and calibrated against boreholes where available; radargrams were interpreted using radar-facies criteria. Comparing the apparent velocity of each hyperbola with the ground velocity separated buried objects from reflections off above-ground structures. The reinforced-concrete slope protection and tailrace lining produced continuous slab reflections, with no major defects or large voids; however, a 35 m section of the tailrace lining exhibited differential slab settlement. Loosened soil was identified at 0.8-2.0 m beneath the tailrace lining and at 0.9-1.5 m beneath the ravine dam slope protection. Beneath the powerhouse platform, intermittent loosened zones extended to 1.1-1.9 m over about a third of the profiles. The most severe anomalies occurred in the stop-log storage area, where chaotic scattering zones 15-16 m wide below 3.5 m indicate intense loosening and possible voids. No widespread subsurface deterioration was found, but the stop-log storage area requires priority investigation. These results provide a baseline for repeat GPR monitoring.*

Keywords: *ground-penetrating radar; earthfill dam; reinforced-concrete slope protection; soil loosening; hydraulic structures; seismically active region; Kapchagay HPP.*

***Corresponding author**
Gulfairuz Kareken, e-mail: gulfairuz_1997@mail.ru

https://doi.org/10.51488/1680-080X/2026.3-04

ӘОЖ 627.8:621.311.21:550.837.76
ҒТАМР 70.17.29
ҒЫЛЫМИ МАҚАЛА

ҰЗАҚ МЕРЗІМДІ ПАЙДАЛАНУ ЖАҒДАЙЫНДАҒЫ ҚАПШАҒАЙ СЭС КӨТЕРГІШ КОНСТРУКЦИЯЛАРЫНЫҢ ТЕХНИКАЛЫҚ ЖАЙ-КҮЙІН ГЕОРАДИОЛОКАЦИЯЛЫҚ ДИАГНОСТИКАЛАУ

Г.Т. Қарекен[1]*, Ж.Н. Молдамуратов[1], Н.И. Ватин[2], Н.А. Шаншабаев[1,3], А.А. Брянцев[1,4], С.Е. Оразов[1]

[1]Халықаралық білім беру корпорациясы, 050043, Алматы, Қазақстан
[2]Ұлы Петр атындағы Санкт-Петербург политехникалық университеті (СПбПУ), 195251, Санкт-Петербург, Ресей
[3]«СтройТехЭкспертиза» ЖШС, Тараз, Қазақстан
[4]«RAS Engineering» ғылыми-зерттеу институты ЖШС, Алматы, Қазақстан

Аңдатпа. *Ұзақ мерзімді пайдалану барысында гидротехникалық құрылыстар мен олардың топырақ негіздерінің күйі нашарлайды, бұл көбінесе сырттан көрінбейтін жасырын ақаулар түрінде дамиды. Зерттеуде сейсмикалылығы 8 балл аймақта 50 жылдан астам пайдаланылып келе жатқан Ш. Чокин атындағы Қапшағай СЭС (Қазақстан) құрылыстарының жер асты күйі георадиолокация (GPR) әдісімен бағаланды. 150 және 400 МГц антенналары бар «ОКО-3» георадарымен алты элементте 62 жазба алынды: станция маңындағы алаң, ағызу каналының қаптамасы, арналық және сай бөгеттерінің жоғарғы беткейлерінің бекітпесі, АТҚ-220 кВ алаңы және шандор қоймасы. Толқындардың таралу жылдамдықтары дифракция гиперболалары бойынша анықталып, мүмкін болған жерлерде ұңғыма деректері бойынша калибрленді; радарограммалар толқындық бейненің сипаты бойынша – синфазды осьтердің конфигурациясы, амплитудасы және созылуы бойынша түсіндірілді. Әрбір гиперболаның көрінерлік жылдамдығын топырақтағы толқын жылдамдығымен салыстыру жер асты объектілерін жер үсті құрылыстарынан болатын шағылысулардан ажыратуға мүмкіндік берді. Беткейлердің темірбетон бекітпесі мен канал қаптамасы плиталардан үздіксіз шағылысулар берді, елеулі ақаулар мен ірі қуыстар анықталған жоқ; алайда канал қаптамасының 35 м учаскесінде плиталардың біркелкі емес шөгуі тіркелді. Тығыздығы төмендеген топырақ канал қаптамасының астында 0,8-2,0 м, сай бөгеті беткейі бекітпесінің астында 0,9-1,5 м тереңдікте анықталды. Станция маңындағы алаң астында тығыздығы төмендеген үзік-үзік аймақтар 1,1-1,9 м тереңдікке дейін таралып, профильдер ұзындығының шамамен үштен бірін алып жатыр. Ең елеулі аномалиялар шандор қоймасында тіркелді: мұнда 3,5 м-ден терең жердегі ені 15-16 м хаостық шашырау аймақтары топырақ тығыздығының қарқынды төмендегенін және қуыстардың болуы мүмкін екенін көрсетеді. Кең ауқымды жер асты бұзылулары анықталған жоқ. Алынған нәтижелер қайталама георадарлық мониторинг үшін бастапқы база болып табылады.*

Түйінді сөздер: *георадиолокация; топырақ бөгеті; еңістердің темірбетон бекітпесі; топырақтың борпылдақтануы; гидротехникалық құрылыстар; сейсмикалық белсенді аймақ; Қапшағай СЭС.*

***Автор-корреспондент**
Гүлфайруз Қарекен, e-mail: gulfairuz_1997@mail.ru

https://doi.org/10.51488/1680-080X/2026.3-04

УДК 627.8:621.311.21:550.837.76
МРНТИ 70.17.29
НАУЧНАЯ СТАТЬЯ

ГЕОРАДИОЛОКАЦИОННАЯ ДИАГНОСТИКА ТЕХНИЧЕСКОГО СОСТОЯНИЯ НЕСУЩИХ КОНСТРУКЦИЙ КАПШАГАЙСКОЙ ГЭС В УСЛОВИЯХ ДЛИТЕЛЬНОЙ ЭКСПЛУАТАЦИИ

Г.Т. Карекен[1]*, Ж.Н. Молдамуратов[1], Н.И. Ватин[2], Н.А. Шаншабаев[1,3], А.А. Брянцев[1,4], С.Е. Оразов[1]

[1]Международная образовательная корпорация, 050043, Алматы, Казахстан
[2]Санкт-Петербургский политехнический университет Петра Великого (СПбПУ), 195251, Санкт-Петербург, Россия
[3]ТОО «СтройТехЭкспертиза», Тараз, Казахстан
[4]ТОО Научно-исследовательский институт «Ras Engineering» , Алматы, Казахстан

Аннотация. *При длительной эксплуатации гидротехнических сооружений их конструкции и грунтовые основания деградируют, причём дефекты нередко развиваются скрыто, без внешних признаков. В работе методом георадиолокации (GPR) оценено подповерхностное состояние сооружений Капшагайской ГЭС им. Ш. Чокина (Казахстан), эксплуатируемой более 50 лет в зоне сейсмичностью 8 баллов. Георадаром «ОКО-3» с антеннами 150 и 400 МГц получено 62 записи на шести элементах: пристанционной площадке, облицовке отводящего канала, креплении верховых откосов русловой и логовой плотин, площадке ОРУ-220 кВ и шандорохранилище. Скорости распространения волн определены по гиперболам дифракции и, где это было возможно, откалиброваны по данным скважин; радарограммы интерпретированы по характеру волновой картины: конфигурации, амплитуде и протяжённости осей синфазности. Сопоставление кажущейся скорости каждой гиперболы со скоростью волн в грунте позволило отделить подземные объекты от отражений от наземных сооружений. Железобетонное крепление откосов и облицовка канала дают непрерывные отражения от плит; существенных дефектов и крупных пустот не выявлено. Вместе с тем на участке облицовки канала длиной 35 м зафиксирована неравномерная осадка плит. Разуплотнённые грунты залегают на глубине 0,8-2,0 м под облицовкой канала и 0,9-1,5 м под креплением откоса логовой плотины. Под пристанционной площадкой прерывистые зоны разуплотнения распространяются до глубины 1,1-1,9 м и занимают около трети длины профилей. Наиболее значимые аномалии выявлены на шандорохранилище: зоны хаотичного рассеяния шириной 15-16 м на глубине более 3,5 м указывают на интенсивное разуплотнение грунта и возможное наличие пустот. Повсеместного ухудшения подповерхностного состояния не установлено, однако шандорохранилище требует первоочередного обследования. Полученные результаты служат основой для повторного георадарного мониторинга.*

Ключевые слова: *георадиолокация; грунтовая плотина; железобетонное крепление откосов; разуплотнение грунта; гидротехнические сооружения; сейсмо активный регион; Капшагайская ГЭС.*

***Автор-корреспондент**
Гульфайруз Карекен, e-mail: gulfairuz_1997@mail.ru

https://doi.org/10.51488/1680-080X/2026.3-04

1 INTRODUCTION

Hydraulic structures, including dams, spillways, intake works and their appurtenant elements, form the backbone of hydropower generation and water-resource management worldwide. Their safe operation is a precondition for energy security and for the protection of downstream population centres. Many large dams in Central Asia were built in the 1960s-1980s and have been in service for 40 to more than 60 years; the Kapchagay HPP, commissioned in 1970, is one of them. Ageing of structural materials, cumulative fatigue under cyclic loading, and gradual degradation of protective linings and facings are therefore a growing concern for dam-safety authorities worldwide. The problem becomes acute where ageing infrastructure coincides with an active seismic environment, because seismic loading can trigger sudden failure in a structure whose safety margin has already been eroded by a slowly developing, latent defect.

The Almaty region, where the Kapchagay Hydropower Plant (HPP) is located, lies at the northern margin of the Tien Shan orogenic belt, a tectonically active intracontinental orogen driven by the ongoing India-Eurasia collision [1, 2]. The region has repeatedly experienced destructive earthquakes. These include the 1885 Belovodskoe (M_w 7.6, an uncertain estimate), 1887 Verny (M_w 7.7) and 1889 Chilik (M_w 7.9) events, whose magnitudes have been re-estimated from magnetogram records [1]. The largest and best-documented event of this series is the 1911 Kebin (Chon-Kemin) earthquake, the strongest instrumentally recorded earthquake in the Tien Shan (M_w 8.0 from teleseismic records [1]; M_w 7.8-7.9 from the geological moment [3]), which produced a cumulative surface rupture exceeding 155-195 km along 13 fault patches grouped into six sections [3].

Figure 1 - General view of the Sh. Chokin Kapchagay HPP: powerhouse and tailrace channel, looking downstream along the Ili River [from open sources]

The Kapchagay dam has recently been monitored instrumentally in this seismic setting: during the 4 March 2024 earthquake (MPV 6.1 in the national catalogue; epicentre about 31 km south of Almaty; focal depth 10 km), the peak acceleration at the rock reference point was 8.10 cm/s² (≈0.0083 g), and crest-to-reference PGA ratios of 0.62-0.70 indicated a low-strain response of the dam-foundation system [4]. Such records characterise weak motion only. According to the detailed seismic zoning of the Almaty region, calculated peak ground accelerations (PGA) for a 2% probability of exceedance in 50 years (2475-year return period) range from 0.4 to 0.9 g over a significant part of the region; the most hazardous zones are concentrated in its southern and south-eastern parts along the ranges of the Northern Tien Shan, where PGA reaches 0.8-0.9 g (MSK-64 intensity 9-10), whereas the central part of the region, including the Kapchagay area, is assessed as a zone of moderate hazard with PGA of 0.3-0.5 g [5]. The recorded 2024 motion was thus less than 3% of the lower bound of the hazard-level PGA for the site. The moderate rating does not, however, remove the regional source

https://doi.org/10.51488/1680-080X/2026.3-04

hazard. Along the Zailisky Alatau rangefront, fault scarps ~2 to >20 m high in alluvial fans record surface-rupturing earthquakes since the Last Glacial Maximum, with minimum estimated magnitudes of M 6.8-7; radiocarbon-dated uplifted river terraces in the eastern section of the rangefront fault indicate a Holocene slip rate of ~1.2-2.2 mm/yr, and active deformation is laterally distributed, affecting the rangefront, the interior of the range and the foreland of the Kazakh platform [6]; In the adjacent northern Tien Shan of Kyrgyzstan (Kyrgyz and Kastek ranges, Chu basin and northern Issyk-Kul area), tectonophysical zoning of active faults based on Coulomb stress reconstructed from earthquake focal mechanisms has identified potentially hazardous fault segments up to 25 km long at several separate locations, capable of generating M 5.5-7.0 events, indicating that critical stress is distributed across the fault system rather than concentrated along a single source [7].

The region continues to register earthquakes of engineering significance. The 4 March 2024 earthquake (MPV 6.1) produced a measurable response at the dam crest, recorded by the plant's engineering-seismometric station [4]. Therefore, structures in the region must be designed and assessed for rare design-basis and maximum-considered earthquakes. They must also withstand the recurrent moderate shaking they experience throughout their service life.

The Sh. Chokin Kapchagay HPP is located on the Ili River at the entrance to the Kapchagay Gorge, approximately 70 km north of Almaty, in the city of Konaev (formerly Kapchagay) (Fig. 1). Construction began in 1965; the first two of the four hydro-units were commissioned at the end of 1970 and the remaining two in 1971, and construction was completed in 1980. The installed capacity of the plant is 364 MW. The hydraulic complex comprises tailwater, headwater and pressure-front structures (Table 1), including the powerhouse, the intake structure, the service spillways, the drainage gallery, the tailrace channel with its reinforced-concrete lining, the 220 kV outdoor switchyard platform and two stop-log storage areas. The pressure front consists of two earthfill dams separated by a natural rock outcrop (Fig. 2). The river-bed (channel) dam is a hydraulic-fill structure 52.0 m high, of which 49.0 m is hydraulically placed fine aeolian sand, and 470.0 m long at the crest. The ravine (saddle) dam, which closes a natural depression on the reservoir rim, is an earthfill embankment with an upstream low-permeability sandy-loam facing; it is 56.0 m high (measured from the base of the facing) and 370.0 m long at the crest. The upstream slopes of both dams are protected by cast-in-place reinforced-concrete slabs (10 × 10 m): 0.20–0.30 m thick above el. 472.0 m on the river-bed dam, and 0.20 m thick from el. 476.96 m up to the crest on the ravine dam.

Table 1 - Structural inventory of the Kapchagay HPP hydraulic complex [Author's material]

Group	Structures
Downstream-pool structures	Powerhouse; drainage gallery; retaining/catch wall behind powerhouse; operations building; tailrace stilling-basin slab; downstream stop-log storage; RC tailrace-canal lining; channel-dam drainage collector; cable tunnel to the 220 kV switchyard; 220 kV switchyard platform; left-bank RC tailrace-canal wall; spillway outlet portal; RC slope revetment of the spillway tailrace canal; HPP tailrace canal; spillway tailrace canal; administrative building; powerhouse foundation-drain collector
Upstream-pool structures	Spillway inlet-head portals No. 1 and No. 2; HPP intake structure; service spillway; intake stop-log storage; spillway approach canal
Pressure-front structures	Channel (river-bed) dam; rock outcrop; the ravine dam

https://doi.org/10.51488/1680-080X/2026.3-04

Figure 2 - Aerial view of the Kapchagay HPP hydraulic complex and its general structural layout [Author's material]

The Kapchagay HPP is a pressing case in this context. Its principal hydraulic structures have been in service for more than 50 years under operational loading and repeated seismic shaking. The dams were originally designed for a seismic intensity of 7; after the seismic zoning maps were revised following the 1988 Spitak earthquake, the seismicity of the site was raised to intensity 8 on the MSK-64 scale, as confirmed in the plant's 2016 safety declaration, and the stability of the dam slopes has since been verified for the design earthquake of intensity 8. Under the Kazakhstan building code SN RK 3.04-01-2023, the class of a main hydraulic structure is determined by its height and foundation type, its socio-economic importance and the consequences of a potential hydrodynamic accident, and is taken as the highest of the resulting classes. Seismic design in Kazakhstan is currently governed by the code of practice SP RK 2.03-30-2017 “Construction in Seismic Zones”, which sets the seismic hazard of construction sites and the design seismic loads. By height and foundation type (52 m and 56 m, on rock foundations), both dams would fall into Class II. However, the reservoir volume (18.6 km^3) and the consequences of a dam failure, with more than 3,000 permanent residents in the potential inundation zone, place both dams in Class I, the highest class of hydraulic structures. Because both dams are Class I structures in a zone of seismic intensity 8, the current code requires seismometric monitoring of the structures, seismological observations and dynamic testing (SN RK 3.04-01-2023, clause 6.5.4).

A companion seismic-monitoring study of paired accelerograph records obtained at a rock reference point and at the dam crest during the 4 March 2024 earthquake (MPV 6.1 in the national catalogue) [4] showed that, although peak crest accelerations were 30-38% lower than at the reference point, the transverse component exhibited frequency-selective amplification at about 1.6 Hz, consistent with the previously reported fundamental frequency of the dam-foundation system (1.5-1.7 Hz), and a secondary amplification band at about 3.6 Hz. The dam-foundation system therefore does not transmit the incoming motion uniformly but amplifies certain frequency components while attenuating others. This finding matters for an ageing structure. In March 2024, the Voroshilov Dam in the same region failed. InSAR and GPR investigations attributed the failure to chronic seepage with developing internal erosion, combined with soil instability, microseismicity and structural wear [5, 8]. It is therefore necessary to establish whether loosening, seepage or voids are already developing in the Kapchagay dams and their reinforced-concrete facings and linings. Such defects could interact adversely with future strong shaking. This interaction has been demonstrated experimentally. In centrifuge tests on a small homogeneous reservoir dam, seismic loading increased the crest crack depth by 11.3-24 times [9]. Subsequent seepage extended the crack to 73.3% of the dam height [9]. The earthquake had therefore weakened the dam body and made it vulnerable to seepage-driven crack propagation.

During the multifactor survey of the Kapchagay HPP, the principal potential causes of defects

https://doi.org/10.51488/1680-080X/2026.3-04

and deterioration of the structural elements were identified. Four of them are relevant to the subsurface condition assessed in this study: (1) physical wear and ageing of structures and materials; (2) seasonal filling and drawdown of the reservoir, with the associated changes in load; (3) damage to and deformation of linings and slope protection; and (4) deterioration of concrete through leaching, seepage and related processes. Items (1), (2) and (4) are physical mechanisms, and item (3) describes their consequences for the linings and slope protection. In a seismically active region, these mechanisms can act together with seismic loading. Repeated seismic loading combined with seepage and progressive soil loosening has been identified as the cause of a recent earthfill dam failure in the Almaty region [5, 8]. GPR profiling addresses the subsurface expression of these processes: loosening related to ageing (1) and load changes (2), deformation of linings (3), and seepage and moisture (4).

The dams are monitored by several complementary means. Settlement observations on the dams and the rock outcrop began in 1976. A piezometric network and a V-notch weir complement them; the weir measures seepage from the drainage system of the ravine dam. Piezometric levels were measured manually until 2017. Since then, an automated safety-monitoring system has been in operation. It comprises 51 BD Sensors LMP 307i pressure transducers in the piezometers of the river-bed dam, the ravine dam and the rock outcrop. It also includes two pressure sensors in the drainage adit, six automated crack meters in the powerhouse and at the intake, and two ultrasonic water-level gauges in the headwater and tailwater. Data are transmitted online to the dispatcher station of the plant. However, the survey found 23 of the 51 pressure transducers, both water-level gauges and one crack meter out of service. The communication line to the tailwater gauge was broken. The instrumental record is therefore long but not continuous. It cannot by itself confirm or rule out newly identified anomalies. Together with visual and geophysical surveys, these observations form part of the annual multifactor survey (MFS). For hydraulic structures in operation for more than 25 years, the national building code requires a comprehensive assessment of strength, stability and operational reliability at least once every five years [10].

GPR has been applied to both concrete and embankment dams. In a large concrete spillway, high-frequency stepped-frequency GPR identified more than 150 anomalies consistent with delamination and voids [11]. Hammer and drilling tests confirmed only part of them, and several deeper anomalies proved to be weathered rock at the concrete-rock interface [11]. On an embankment dam, GPR combined with thermal imaging found no active seepage paths [12]. It did, however, reveal shallow deformation of the upstream face, affecting the asphalt facing and the underlying layers to several metres depth [12]. More recently, a 200 MHz GPR survey of the crests of a concrete arch dam and a rockfill dam in Romania identified near-surface deformation and rebar degradation [13]. These results complemented routine geodetic monitoring. In Kazakhstan, satellite radar interferometry (InSAR) revealed a persistent multi-year increase in deformation of the Voroshilov Dam before its failure in March 2024 [8]. GPR surveys after the reservoir was drained showed abnormally high moisture throughout the dam body, indicating long-term seepage and internal erosion [8]. Other Kazakh studies have addressed GPR detection of hidden defects [14], multifactor assessment of a reservoir in a seismically active zone [15], degradation of concrete hydraulic structures [16] and reservoir reconstruction [17]. However, to the authors' knowledge, most published case studies address a single structure. Few cover all principal elements of a multi-structure hydropower complex in one survey campaign. Fewer still combine GPR with the other components of a statutory multifactor survey: visual inspection, geodetic observations and piezometric monitoring.

An undetected defect that develops over time could compromise the structural integrity of the dams. Such defects include age-related decompaction of the fill, internal seepage, voids beneath the reinforced-concrete slope protection and loss of slope stability under seismic loading. Their consequences would affect the population of the downstream inundation zone, the plant personnel and the operation of the plant. Timely detection through systematic, repeated surveys allows remedial measures to be planned while the structures remain serviceable. A developing defect can then be addressed through planned maintenance rather than emergency intervention.

This study presents a GPR assessment of six structural elements of one hydropower complex that includes two Class I earthfill dams. Five of these elements are surveyed by GPR within the annual

https://doi.org/10.51488/1680-080X/2026.3-04

multifactor survey. The sixth, the stop-log storage area, was added because ground subsidence had been observed there. The GPR results for each element are compared with the findings of the multifactor survey, in which the authors participated. The study thus provides a published reference dataset for repeated surveys of ageing hydraulic structures in a seismically active region of Kazakhstan.

The novelty of the study is threefold. First, to the authors' knowledge, it is the first peer-reviewed GPR-based condition assessment of all principal structures of the Kapchagay HPP. This Class I hydraulic complex has been in service for more than 50 years in a seismically active region. Second, all six elements were surveyed with the same GPR system and processed with a consistent workflow. The elements range from the reinforced-concrete slope protection of a hydraulic-fill dam of fine aeolian sand to the plant platforms and the tailrace lining. This allows the type and extent of subsurface anomalies to be compared across elements that differ in design, fill material and loading. Third, the GPR anomalies are cross-checked against visual observations, observed ground subsidence and borehole data from the multifactor survey. The indications of voids, decompaction and elevated moisture are therefore not inferred from radargrams alone. The results also complement the seismic monitoring of the same structures reported in [4].

The aim of the study is to assess the current condition of the hydraulic structures of the Kapchagay HPP by GPR profiling. The specific objectives are (i) to identify zones of deterioration, reduced compaction, elevated moisture and possible voids, and to compare their distribution across the six structural elements; and (ii) to formulate conclusions and recommendations for the continued safe operation of the plant.

The paper first describes the physical principle of GPR, the equipment and the survey configuration. It then presents the results for six elements: the powerhouse platform, the reinforced-concrete lining of the tailrace channel, the upstream slope protection of the river-bed dam and the ravine dam, the 220 kV outdoor switchyard platform and the stop-log storage area. The paper closes with the findings and recommendations.

2 MATERIALS AND METHODS

2.1 Physical Principle of GPR Measurements

GPR emits short (nanosecond) electromagnetic pulses with wavelengths from decimetres to metres (Fig. 3). The pulses are reflected at interfaces between materials with different dielectric permittivity and, to a lesser extent, electrical conductivity. Water ($\varepsilon \approx 81$) and air ($\varepsilon \approx 1$) differ most in permittivity among the common constituents of near-surface materials. Water content therefore largely controls the bulk permittivity of a layer. Dry, massive materials have low permittivity and high wave velocity, whereas saturated materials have high permittivity and low velocity [18]. The radar measures the two-way travel time t, which is converted into the depth h of a reflector as Eq.(1) and (2):

$$h = \frac{vt}{2} \tag{1}$$

$$v = \frac{c}{\sqrt{\varepsilon}} \tag{2}$$

where v is the propagation velocity in the medium, $c \approx 0.3$ m/ns is the velocity in free space and ε is the relative permittivity [18].

https://doi.org/10.51488/1680-080X/2026.3-04

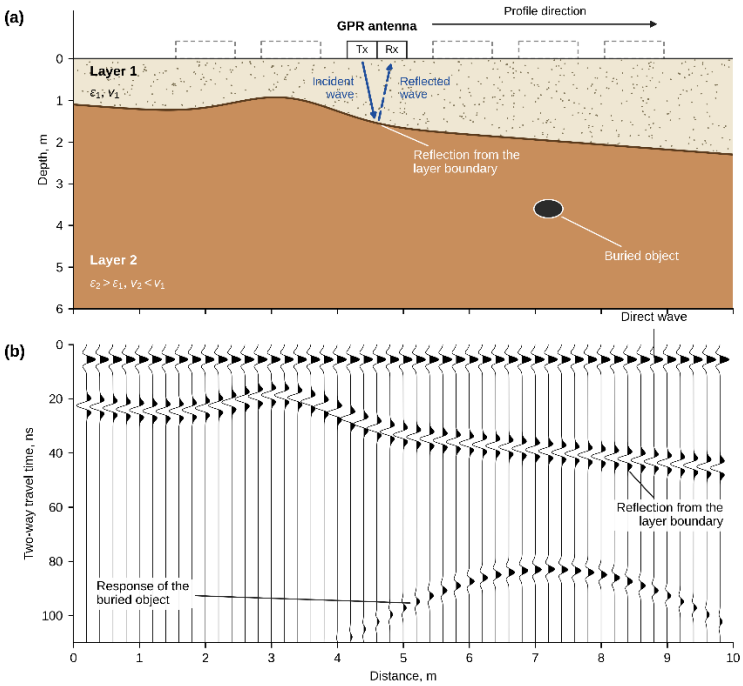

Figure 3 - Basic operating principle of ground-penetrating radar: (a) geological section with the GPR antenna, two layers of different permittivity ($\varepsilon_2 > \varepsilon_1$) and a buried object; (b) synthetic traces (150 MHz wavelet) showing the direct wave, the reflection from the layer boundary and the diffraction hyperbola from the object. Schematic with illustrative values [Author's material]

An object comparable to or smaller than the wavelength in the host medium acts as a point scatterer. It produces a diffraction hyperbola in the radargram (Fig. 4). The apex of the hyperbola marks the position of the object, and the curvature of its limbs gives the wave velocity in the host material [19]. Such hyperbolae are produced by objects with contrasting dielectric properties, such as construction debris, boulders and voids [19].

In this study, the wave velocity was determined from well-defined diffraction hyperbolae at different time levels. Where borehole data were available, the velocity was calibrated against them. At the powerhouse platform, boreholes had been drilled during earlier surveys. There, the velocity was about 0.10 m/ns, corresponding to $\varepsilon \approx 9$ by Eq. (2). This value was used for time-to-depth conversion by Eq. (1). The average velocities for the other elements were about 0.10 m/ns ($\varepsilon \approx 9$) for the river-bed dam facing, about 0.085 m/ns ($\varepsilon \approx 12$) for the tailrace lining, the ravine dam facing and the switchyard, and about 0.15 m/ns ($\varepsilon \approx 4$) for the dry fill of the stop-log storage area.

https://doi.org/10.51488/1680-080X/2026.3-04

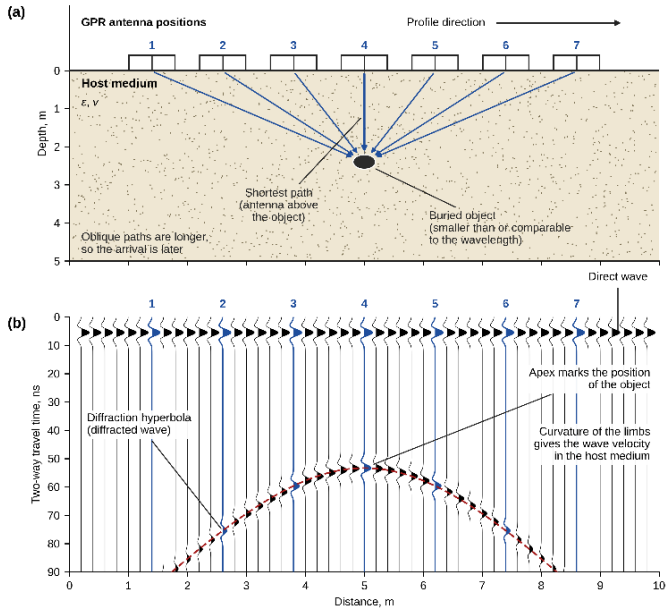

Figure 4 - Formation of a diffraction hyperbola from a discrete buried object as the antenna moves along the profile: (a) ray paths from successive antenna positions (1-7) to the object; (b) synthetic traces (150 MHz wavelet) at the same positions (highlighted in blue) showing the direct wave and the diffracted wave, whose arrival times form a hyperbola. Schematic with illustrative values [Author's material]

2.2 GPR Equipment

Measurements were made with the OKO-3 GPR system (Logical Systems LLC, Russia; Fig. 5). The system consists of a shielded antenna unit with transmitting and receiving antennas, a distance sensor and a control/recording unit. Two interchangeable antenna units were used. The AB-150M has a central frequency of 150 MHz and a nominal sounding depth of 12-16 m. The AB-400M has a central frequency of 400 MHz and a nominal sounding depth of 5-10 m. Penetration decreases in moist or clayey materials. In this survey, the recording time windows limited the depth of investigation to about 6-7 m. Table 2 lists the specifications of the AB-150M unit.

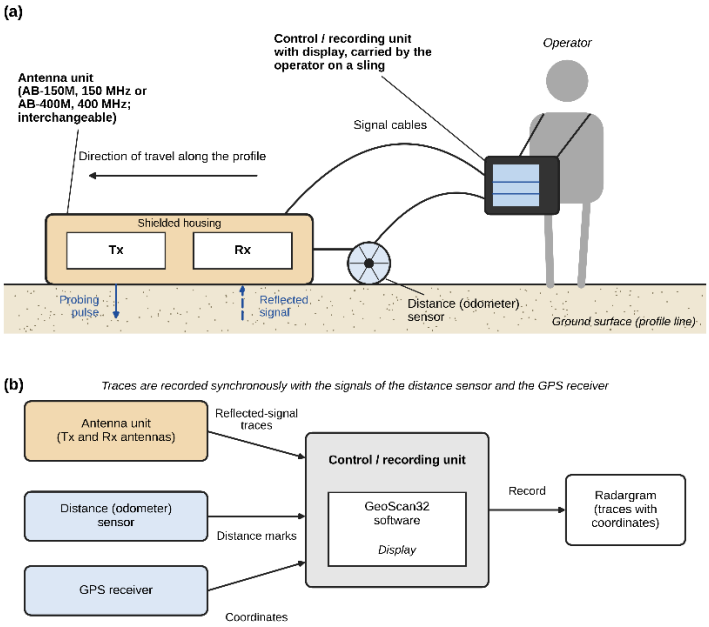

Figure 5 - OKO-3 ground-penetrating radar: (a) field configuration, in which the shielded antenna unit (transmitting, Tx, and receiving, Rx, antennas) is moved along the profile, the distance sensor triggers the recording, and the control/recording unit is carried by the operator on a sling; (b) data-acquisition scheme. [Author's material]

https://doi.org/10.51488/1680-080X/2026.3-04

Table 2 - Principal technical specifications of the OKO-3 GPR system with the AB-150M antenna unit [Author's material]

Parameter	Value
Central frequency (AB-150M)	150 MHz ± 30%
Transmitter pulse amplitude (AB-150M)	≥ 500 V
Receiver sensitivity (all antenna units)	≤ 300 μV
Supply voltage	12 V ± 20%
Continuous operating time	≥ 4 h
Nominal sounding depth (AB-150M)	12–16 m
Depth resolution (AB-150M)	0.35 m

2.3 Survey Objects and Data Acquisition

The survey covered six structural elements: the powerhouse platform, the reinforced-concrete lining of the right bank of the tailrace channel, the upstream slopes of the river-bed dam and the ravine dam, the 220 kV switchyard platform and the stop-log storage area. The first five are surveyed annually within the multifactor survey. The stop-log storage area was added because ground subsidence had been observed there. Visual inspection related the subsidence to surface water from rainfall and snowmelt entering a vertical cavity near a support post. The cavity had formed at the contact between the reinforced-concrete and soil cover of the site. The survey archive contains 62 records, numbered as radargrams Nos. 1-60 because Nos. 22 and 53 were each assigned to two records. Profile numbers are field designations and do not coincide with radargram numbers.

- Powerhouse platform (radargrams Nos. 1-18): nine longitudinal profiles (001-009, about 30-40 m) and nine transverse profiles (0010-0018, about 30-35 m). The profiles cover the ground around the powerhouse and the service buildings on the left bank of the tailrace channel, including part of the downstream slope of the river-bed dam.
- Tailrace-channel lining (Nos. 19-22; five records, with No. 22 assigned to Profiles 004 and 005): Profiles 001-005 (50-150 m) on the right-bank reinforced-concrete slabs. The slabs are 0.20 m thick and lie on soil on slopes of 1:2 to 1:1.5 between el. 446.5 and 450.0 m. They were built in 1971 and 1973.
- River-bed dam upstream slope (Nos. 23-30): Profiles 049-056 (about 50-400 m) on monolithic M200 reinforced-concrete slabs, 0.20 and 0.30 m thick, laid on soil. The surveyed facing covers about 32,000 m².
- Ravine dam upstream slope (Nos. 31-45): Profiles 019-033 on the reinforced-concrete facing (M200 slabs, 0.20 and 0.30 m thick, laid on soil) between the crest and the berm.
- 220 kV switchyard platform (Nos. 46-59; 15 records, with No. 53 assigned to Profiles 041 and 042): Profiles 034-048 (35-105 m).
- Stop-log storage area (No. 60): one 105 m record along the line of ground disturbance (Profile 060).

On the dam facings, longitudinal profiles ran parallel to the waterline and transverse profiles perpendicular to it. Positions along a profile are given as chainage (Pk, m). Recording was triggered by the distance sensor, which was synchronised with a GPS receiver. Reference features, such as poles, kerbs, pavement edges and facings, were marked in GeoScan32. Profile positions were tied to the plans of previous surveys. At the powerhouse platform, the profile layout repeated that of the previous survey, which allows direct comparison of results. The time window was 150 ns (95 ns at the storage area). The antenna unit, the number of samples per trace, the stacking and the trace step were set for each element according to the required depth and resolution.

2.4 Data Processing and Interpretation

The data were processed in GeoScan32, GEORADAR-Expert 2.0 and MatGPR. Processing included mean-trace subtraction, gain adjustment and band-pass filtering. The direct wave occupies the uppermost 0-5 ns and is marked as the "visible zone" in the figures. Radargrams are shown in grey scale (Figs. 6 and 7) or in the relative colour palette "degree of compaction" (Figs. 8 and 9). The annotations were made during the field survey.

https://doi.org/10.51488/1680-080X/2026.3-04

Depths were calculated by Eq. (1) with the velocities given above. A single average velocity was applied to each record, so the depth scales are approximate. The 150 ns window corresponds to about 6 m at 0.085 m/ns and about 7 m at 0.10 m/ns. The 95 ns window at the storage area corresponds to about 6 m.

Interpretation followed established radar-facies criteria [20]:

- a continuous high-amplitude reflector at the top of the section represents the asphalt or concrete slab; its undulation, offset or break indicates a defect of the slab or of its contact with the base;
- a chaotic, disrupted, high-amplitude pattern with irregular in-phase axes indicates reduced compaction (loosening); large chaotic scattering zones indicate distributed loosening or voids;
- zones of elevated moisture were delineated with the weighted water-content attribute;
- hyperbolae with curvature consistent with the ground velocity indicate buried objects: sparse, irregular hyperbolae indicate distributed infrastructure, and a single symmetric hyperbola indicates a discrete object;
- broad hyperbolae that imply an apparent velocity well above that of the ground, close to 0.3 m/ns, indicate reflections from above-ground structures;
- fans of dipping hyperbolae on one or both sides of a section indicate lateral reflections from adjacent buildings;
- narrow full-depth bands of high-frequency ringing indicate buried metal ("metal ringing") [21].

For each group of elements, the radargrams with the most distinct diagnostic features were selected for detailed description.

2.5 Attribute Processing

In addition to the visual interpretation, the records were processed in GEORADAR-Expert 2.0 as a semi-automated cross-check. This processing is based on the dependence of wave velocity and amplitude on soil bulk density [22]. Each profile was divided into 10-50 m segments. Filtering, envelope extraction, smoothing or Fourier transformation and trend removal were applied, and the backscattered electromagnetic field (BSEF) was analysed. Two attribute sections were derived. The Q-factor section is based on histograms of the ratio of the central frequency of the amplitude spectrum to its bandwidth. It served as a proxy for soil loosening, with lower values indicating stronger scattering in loosened material. The weighted water-content section served as a proxy for elevated moisture. The attribute sections were used only to support the visual interpretation of loosening and moisture zones, and no quantitative attribute statistics are presented.

3 RESULTS AND DISCUSSION

3.1 Powerhouse Platform

Eighteen radargrams were recorded on the powerhouse platform along nine longitudinal (001-009) and nine transverse (0010–0018) profiles. Eight radargrams with the most distinct diagnostic features were selected for detailed analysis. They are described in two groups of four: longitudinal (Fig. 6, Table 3) and transverse (Fig. 7, Table 4). In all records, the asphalt pavement appears as a continuous shallow reflector at the top of the section. Below it, a chaotic, discontinuous reflection pattern with short, irregularly oriented, high-amplitude segments extends to ~1.1-1.8 m depth. Following established radar-facies criteria [20], this pattern is interpreted as reduced compaction (loosening) of the subgrade fill. The interpretation agrees with the field survey, which found crushed-stone and gravel fill and man-made fill with construction debris in the upper part of the section. Most profiles also show sets of parallel, linear dipping events in the deeper part of the section. Their moveout corresponds to an apparent velocity of ~0.3 m/ns, the velocity of electromagnetic waves in air. These events are therefore lateral reflections from adjacent above-ground buildings, not subsurface features.

https://doi.org/10.51488/1680-080X/2026.3-04

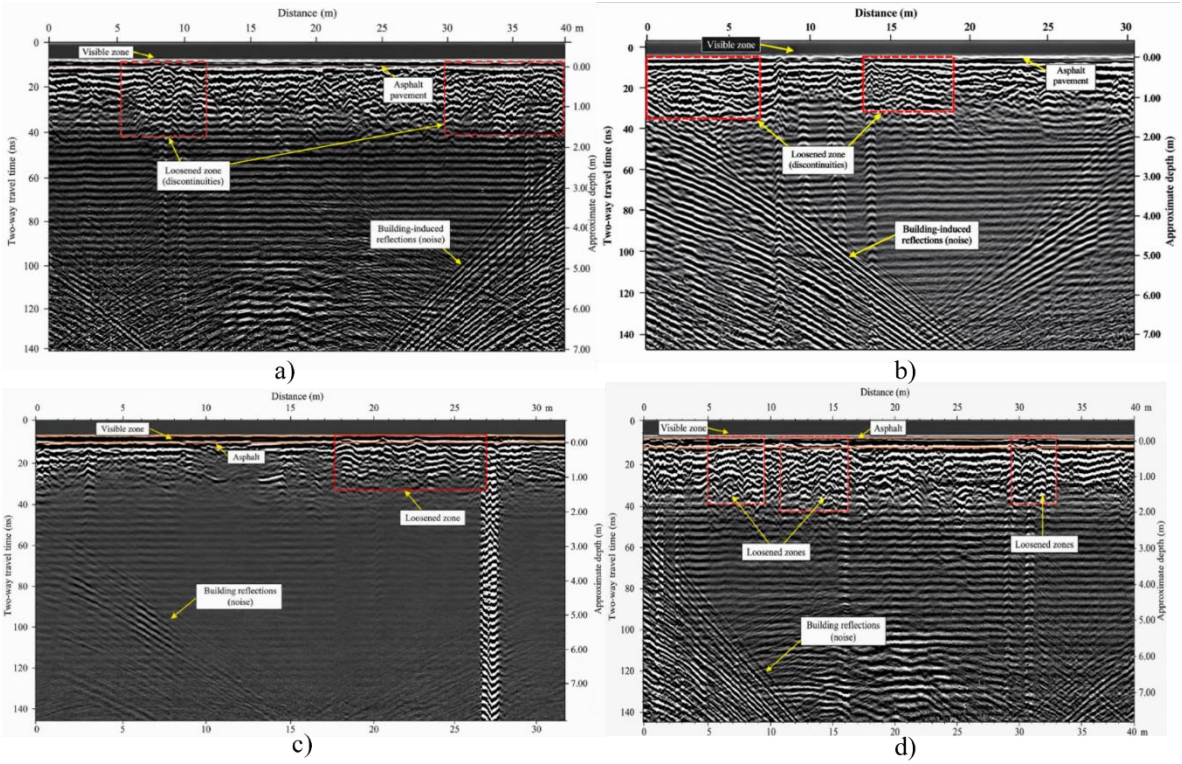

Figure 6 - (a) GPR radargram - Longitudinal Profile 001. (b) GPR radargram - Longitudinal Profile 002. (c) GPR radargram - Longitudinal Profile 004. (d) GPR radargram - Longitudinal Profile 006 [Author's material]

Radargram No. 1 (Profile 001, ~40 m; Fig. 6a) is described in the most detail and serves as the reference for the other profiles. A continuous high-amplitude reflector marks the asphalt along the entire line. Two zones of reduced compaction occur at ~6-12.5 m and from ~31 m to the end of the line. They extend to ~1.7 m and ~1.6 m depth, respectively. The second zone reaches the end of the profile and may continue beyond it. Building-induced dipping events are strongest in the lower right part of the section (beyond ~29 m, below ~3 m). A weaker set appears in the lower left corner (0-8 m, below ~5 m).

Radargram No. 2 (Profile 002, ~30 m; Fig. 6b) shows two zones of reduced compaction, at ~0-6.5 m and ~13-18 m. They extend to ~1.3 m and ~1.1 m depth and show the same reflection pattern as Profile 001. Building-induced dipping events are stronger than on Profile 001 and occur on both sides of the section. They are broad on the left (0-18 m, below ~2 m) and weaker on the right (beyond ~20 m, below ~3.5 m).

Radargram No. 4 (Profile 004, ~30 m; Fig. 6c) shows a single zone of reduced compaction at ~16.5-25.5 m, extending to ~1.2 m depth. Building-induced dipping events are confined to the left side of the section (0-13 m, below ~3 m). At ~25.5-26.5 m, a narrow vertical band of high-amplitude, high-frequency ringing extends through the full depth of the record. This signature is typical of reverberation from a buried metallic object [21]. Similar ringing appears at ~14 m on transverse Profile 0018 (Fig. 7d), near the intersection of the two lines. The ringing masks the underlying reflections, so the boundary of the loosened zone at ~25.5 m cannot be located precisely.

Radargram No. 6 (Profile 006, ~41 m; Fig. 6d) shows three zones of reduced compaction, the largest number among the longitudinal profiles. They occur at ~5-10 m, ~11.5-17.5 m and ~30-34 m and extend to ~1.7, ~1.8 and ~1.5 m depth, respectively. The first two zones are only ~1.5 m apart. They may form a single disturbance that appears segmented because of local variations in the reflected signal. Building-induced dipping events are strong on the left (0-10 m, below ~2 m) and weak in the lower right corner (beyond ~35 m, below ~6 m).

https://doi.org/10.51488/1680-080X/2026.3-04

Table 3 - Comparative summary of longitudinal GPR profiles at the power-station platform (Profiles 001, 002, 004, 006) [Author's material]

Profile (Fig.)	Length	Compaction-loss zones	Building interference	Notable feature
001 (Fig. 6 (a))	40 m	Two zones, ~6-12.5 m and ~31 m to end of line (to ~1.7 and ~1.6 m depth); ~39% of profile length	Strong on the right (>29 m); weaker in the lower left (0-8 m)	Reference record; second zone may continue beyond the line
002 (Fig. 6 (b))	30 m	Two zones, ~0–6.5 m and ~13-18 m (to ~1.3 and ~1.1 m depth); ~38%	Both sides: broad on the left (0-18 m); weaker on the right (>20 m)	Strongest building interference of the four records
004 (Fig. 6 (c))	30 m	Single zone, ~16.5-25.5 m (to ~1.2 m depth); ~30%	Left side (0-13 m)	Narrow full-depth vertical band (~25.5–26.5 m), classified as metal ringing
006 (Fig. 6 (d))	41 m	Three zones, ~5-10, ~11.5-17.5 and ~30-34 m (to ~1.7, ~1.8 and ~1.5 m depth); ~37%	Both sides: strong on the left (0-10 m), weak in the lower right corner (>35 m)	First two zones, ~1.5 m apart, may form one disturbance

All four longitudinal profiles show the same signature of compaction loss: a chaotic, discontinuous, high-amplitude pattern within the upper ~1.1-1.8 m (Table 3). This anomaly type is consistent across the platform and is not confined to individual profiles. The number of zones varies from one on Profile 004 to three on Profile 006. In total, zones of reduced compaction occupy ~36% of the longitudinal profile length (~51 of ~141 m). The share ranges from ~30% on Profile 004 to ~39% on Profile 001. Building-induced interference dominates on the right on Profile 001 and on the left on Profiles 002, 004 and 006. This pattern reflects the position of each survey line relative to the adjacent buildings.

https://doi.org/10.51488/1680-080X/2026.3-04

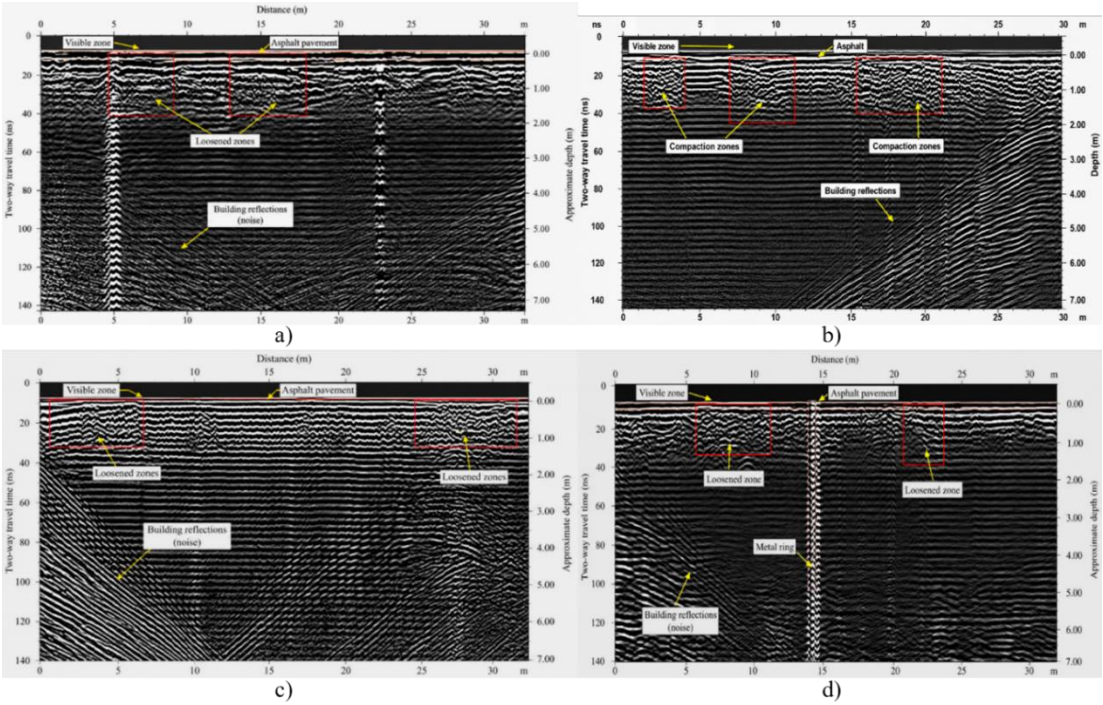

Figure 7 - (a) GPR radargram - Transverse Profile 0010. (b) GPR radargram - Transverse Profiles 0012-0013. (c) GPR radargram - Transverse Profile 0016. (d) GPR radargram - Transverse Profile 0018 [Author's material]

Radargram No. 10 (Profile 0010, ~32 m; Fig. 7a) is the first transverse profile, oriented perpendicular to the longitudinal lines. It shows two zones of reduced compaction, at 4-8.5 m and ~12.5-17.5 m, extending to ~1.6 m and ~1.5 m depth. Their reflection pattern matches that of the longitudinal profiles. Two narrow vertical ringing bands are also present. The first, at ~4 m, is strong and extends through the full depth of the record. The second, at ~21 m, is weaker and discontinuous and is most distinct in the upper ~3 m. Both resemble the metal-ringing band on Profile 0018 and are attributed to buried metallic objects. The band at ~4 m coincides with the edge of the first zone, so this boundary cannot be located precisely. Building-induced dipping events occupy the lower part of the section, below ~4 m.

Radargram No. 13 (Profiles 0012-0013, ~34.5 m; Fig. 7b) shows three zones of reduced compaction, at 2-5 m, ~8-13 m and ~18-24.5 m. They extend to ~1.4, ~1.9 and ~1.6 m depth, respectively. Building-induced dipping events occupy the right-hand part of the section, beyond ~18 m and below ~2.5 m.

Radargram No. 16 (Profile 0016, ~32 m; Fig. 7c) shows two zones of reduced compaction, at ~0.5-4.5 m and ~24.5-30.5 m, extending to ~1.2 m and ~1.5 m depth. Building-induced dipping events are strong in the lower left part of the section (0-10 m, below ~2 m) and weaker in the lower right corner. The interference is thus two-sided, as on longitudinal Profiles 002 and 006.

Radargram No. 18 (Profile 0018, ~32 m; Fig. 7d) shows two zones of reduced compaction, at ~6-11 m and ~20-22.5 m, extending to ~1.2 m and ~1.6 m depth. A narrow, full-depth, high-amplitude vertical band occurs at ~14 m. It is the only band in the dataset labelled in the field records as metal ringing, i.e. reverberation from a buried metallic object [21]. The similar bands on Profiles 004 and 0010 are therefore assigned to the same type of anomaly. Their origin has not been verified by excavation. Building-induced dipping events occupy the lower left part of the section (0-10 m, below ~3 m).

Table 4 - Comparative summary of transverse GPR profiles at the power-station platform (Profiles 0010, 0012–0013, 0016, 0018) [Author's material]

Profile (Fig.)	Length	Compaction-loss zones	Building interference	Notable feature

https://doi.org/10.51488/1680-080X/2026.3-04

0010 (Fig. 7 (a))	~32 m	Two zones, ~4-8.5 m and ~12.5-17.5 m (to ~1.6 and ~1.5 m depth); ~30%	Lower part of the section (below ~4 m)	Two vertical ringing bands: strong, full-depth at ~4 m; weaker at ~21 m
0012–0013 (Fig. 7 (b))	~34,5 m	Three zones, ~2-5, ~8-13 and ~18-24.5 m (to ~1.4, ~1.9 and ~1.6 m depth); ~42%	Right side (>18 m)	Largest share of loosened length and deepest zone (~1.9 m) of the dataset
0016 (Fig. 7 (c))	~32 m	Two zones, ~0.5-4.5 m and ~24.5-30.5 m (to ~1.2 and ~1.5 m depth); ~31%	Both sides: strong, lower left (0-10 m); weaker, lower right	Two-sided interference, as on Profiles 002 and 006
0018 (Fig. 7 (d))	~32 m	Two zones, ~6-11 m and ~20-22.5 m (to ~1.2 and ~1.6 m depth); ~23%	Left side (0-10 m)	Only record with an explicit "metal ringing" label (~14 m)

The transverse profiles confirm the longitudinal results (Table 4). Zones of reduced compaction occupy ~32% of the total transverse profile length (~41.5 of ~130.5 m), compared with ~36% on the longitudinal profiles. The share ranges from ~23% on Profile 0018 to ~42% on Profiles 0012–0013. The zones appear on both orthogonal sets of lines and are therefore distributed across the entire platform. They do not, however, form a continuous layer. On every profile, they alternate with intervals of undisturbed reflections and extend no deeper than ~1.1-1.9 m. This agrees with the field survey, which found weakly consolidated man-made fill at 0.5-1.5 m depth, locally to 2-2.5 m, and no loosening associated with concentrated seepage. The deeper part of this range (2-2.5 m) was not observed on the profiles analysed here.

Three types of anomaly are therefore present on the platform:

(i) zones of reduced compaction within the upper ~2 m;

(ii) building-induced dipping events in the deeper part of the section, on one or both sides depending on the position of the line relative to the buildings;

(iii) narrow, full-depth vertical ringing bands attributed to buried metallic objects.

The survey was conducted in November, after a period of heavy rainfall. A zone of elevated moisture was recorded at 0.3-1.2 m depth over almost the entire platform. Infiltrated rainwater may therefore have increased the reflection amplitudes within the loosened zones.

3.2 Reinforced-Concrete Linings and Facings

The GPR survey of the Kapchagay HPP comprised 62 records across the six structural elements. All records except that of the stop-log storage area cover a time window of ~0-150 ns. With the velocities adopted above, this corresponds to ~6-7 m depth. This section describes four representative records of the reinforced-concrete lining and slope protection (Fig. 8, Table 5). Four records of the switchyard and the stop-log storage area are described in the next section (Fig. 9, Table 6).

https://doi.org/10.51488/1680-080X/2026.3-04

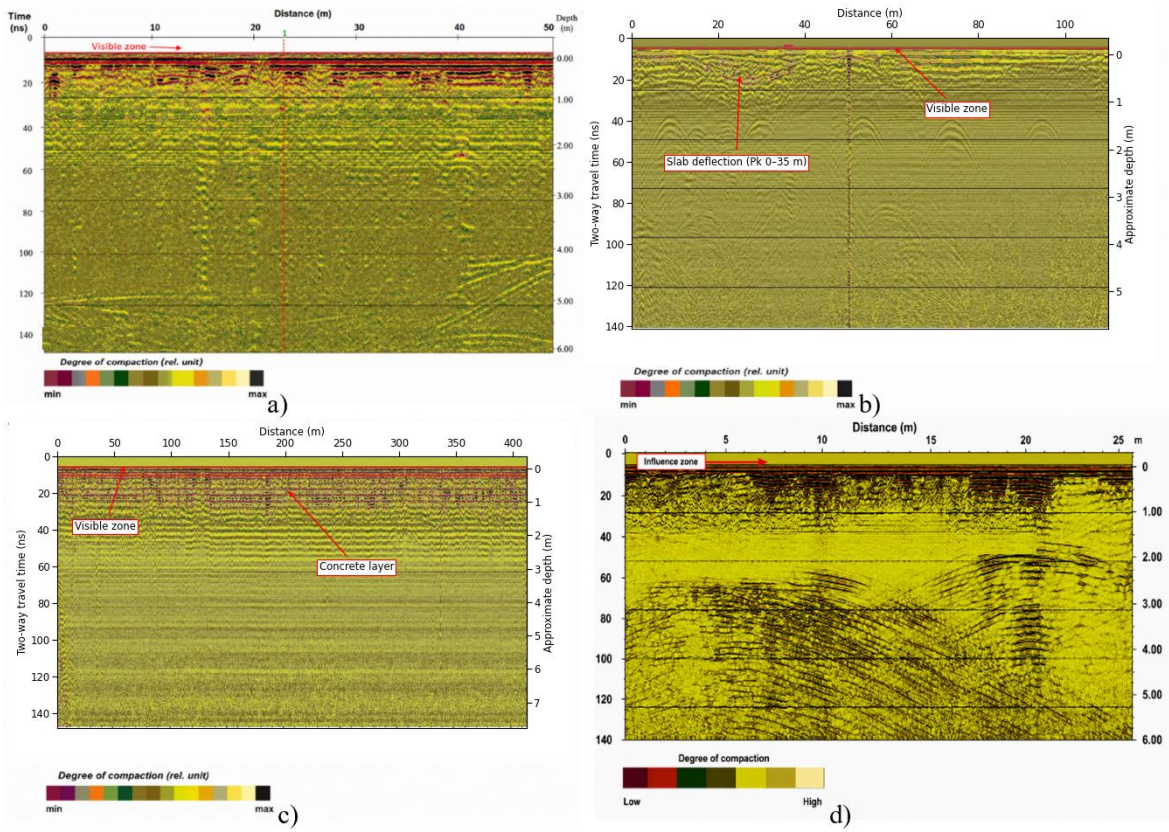

Figure 8 - (a) Interpretation of Radargram No. 19 (Profile 001), tailrace-channel lining, right bank; (b) Interpretation of Radargram No. 21 (Profile 003), tailrace-channel lining, right bank; (c) Interpretation of Radargram No. 23 (Profile 049), river-bed dam, upstream slope; (d) Interpretation of Radargram No. 31 (Profile 019), the ravine dam, upstream slope [Author's material]

Profile 001 (tailrace channel lining, 50 m; ~6 m at v ≈ 0.085 m/ns; Fig. 8a). Below the direct-wave zone (~0-8 ns), a laterally continuous, high-amplitude reflector package occurs at ~8-25 ns. It represents the 0.20 m slab together with reverberation from its reinforcement mesh. The slab thickness is close to the vertical resolution of the antenna. The continuity of the package therefore rules out major discontinuities, but it cannot resolve thin delaminations. Below the package (~25-150 ns), the bedding shows a diffuse, low-coherence texture consistent with reduced-compaction backfill. Field observations located loosened soil beneath the right-bank lining at 0.8-2.0 m depth and elevated moisture at 1.0-2.5 m depth. A set of dipping reflections occurs at Pk ~38-50 m (~100-150 ns; ~4-6 m) and continues to the end of the profile. It is attributed to a buried linear feature or to lateral reflection from an adjacent structure.

Profile 003 (tailrace channel lining, 110 m; ~6 m; Fig. 8b). At Pk ~0-35 m, the lining package (~8-20 ns) is undulating and flexed downward, most clearly at Pk 20-35 m. On the rest of the profile it is planar and laterally continuous. The flexure is interpreted as local differential settlement of the slabs. This agrees with the settlement of the bedding at slab joints and the deformation of the lining surface observed on the right bank of the tailrace channel. The bedding contains isolated diffraction hyperbolae with apexes at ~40 ns (~1.3 m). They occur at Pk ~32, ~64 and ~95 m, at a regular spacing of ~30 m. This regularity suggests periodic structural elements, such as drains or joint details, rather than random inclusions.

Profile 049 (river-bed dam slope protection, ~400 m; ~7 m at v ≈ 0.10 m/ns; Fig. 8c) is the longest profile of the survey. Below the direct-wave zone, a dense, banded, high-amplitude sequence extends to ~20-25 ns. It is marked on the original record as the concrete layer. Because the slabs are only 0.20-0.30 m thick, this sequence includes slab reverberation and the slab-bedding contact. Its amplitude and character are uniform along the entire profile, with no offsets or interruptions. This is consistent with GPR continuity assessments of large concrete structures at other dams [11]. Field

https://doi.org/10.51488/1680-080X/2026.3-04

observations likewise found no slab failure and no cavities beneath the slabs. They recorded only minor loosening of the soil beneath the slabs at 0.9-1.1 m depth and local minor settlement and wetting near the waterline.

Profile 019 (ravine dam slope protection, 26 m; ~6 m at v ≈ 0.085 m/ns; Fig. 8d) is the first record from the ravine dam. The slab appears as a tightly spaced, high-amplitude reflector package to ~20-25 ns. It contains high-amplitude patches at Pk ~5-13 m and ~18-21 m, which indicate local variations in the contact between the slabs and the bedding. Below ~40 ns, broad intersecting hyperbolic events dominate the section. Their curvature is far flatter than that of hyperbolae from buried objects and implies an apparent velocity close to that in air. They are therefore reflections from above-ground objects, not deformation of the bedding. Field observations found minor loosening of the soil beneath the ravine dam slabs at 0.9-1.5 m depth and minor local settlement near the waterline.

Table 5 - Condition of the reinforced-concrete lining and slope protection (Profiles 001, 003, 049, 019) [Author's material]

Profile (Fig.)	Length	Facing/lining continuity	Bedding response	Interpretation
001 (Fig. 8 (a))	50 m	Continuous package, no major discontinuity	Diffuse, reduced compaction; dipping hyperbolic fan at Pk 38-50 m	Lining without major defects; loosening at 0.8-2.0 m depth
003 (Fig. 8 (b))	110 m	Undulating deflection at Pk 0-35 m; continuous beyond	Isolated hyperbolae at ~1.3 m, spaced ~30 m (Pk ~32, ~64, ~95 m)	Local differential settlement of slabs (Pk 0-35 m)
049 (Fig. 8 (c))	≈400 m	Uniform amplitude and character along the entire length	Not differentiated at this scale	No slab failure or cavities; minor loosening at 0.9-1.1 m depth
019 (Fig. 8 (d))	26 m	Continuous; local contact variation (Pk 5-13 m, 18-21 m)	Broad intersecting hyperbolae with near-air apparent velocity	Above-ground reflections; minor loosening at 0.9-1.5 m depth

The four records cover the range of conditions observed on the concrete elements (Table 5). On Profiles 001 and 049, the slab reflector is continuous, with no offsets or loss of amplitude. The river-bed dam slope protection (Profile 049) is the more uniform of the two, whereas the tailrace lining (Profile 001) overlies reduced-compaction bedding. Profile 003 is the only record on which the slab reflector itself is deformed, over ~35 m. This indicates settlement of the slabs, not a feature confined to the bedding. On Profile 019, the slab reflector is continuous but shows local amplitude variations, and the deeper events are unrelated to the subgrade. Because the slabs are only 0.20–0.30 m thick, the records confirm the continuity of the slope protection and the absence of large voids beneath it, but cannot exclude thin delaminations.

https://doi.org/10.51488/1680-080X/2026.3-04

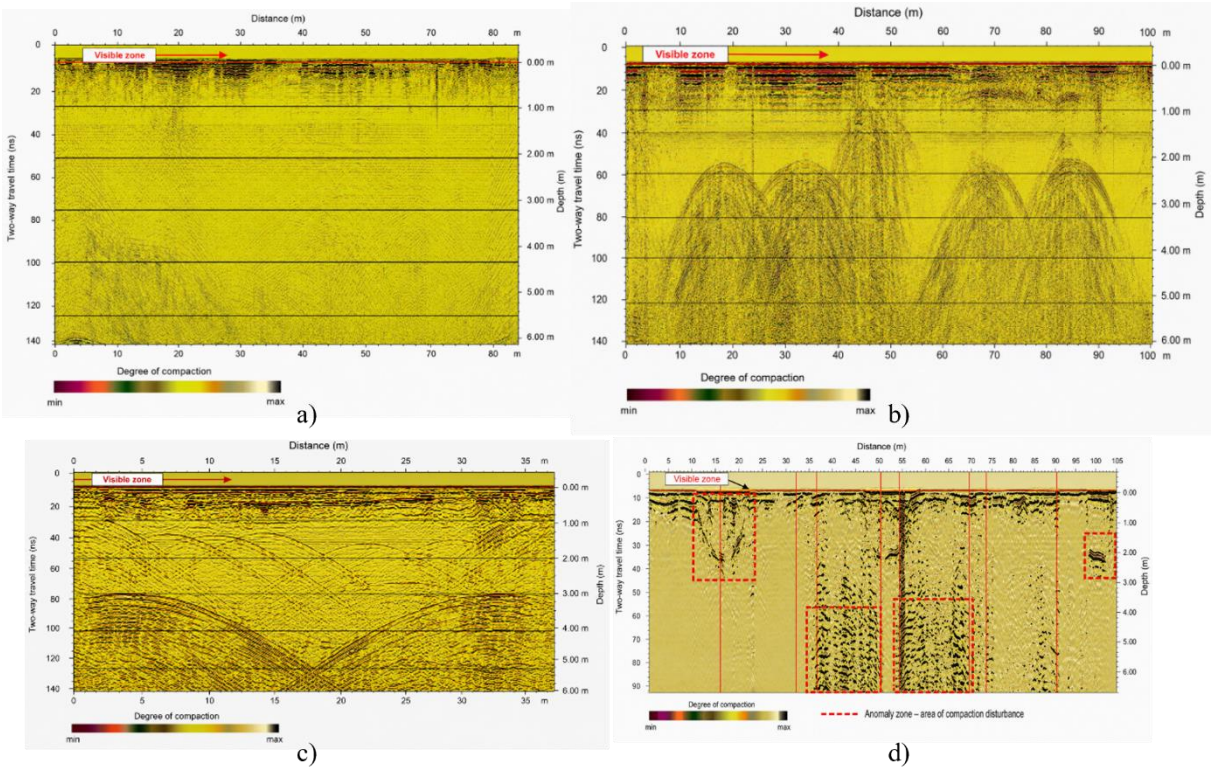

Figure 9 - (a) Interpretation of Radargram No. 46 (Profile 034), 220 kV switchyard platform; (b) Interpretation of Radargram No. 52 (Profile 040), 220 kV switchyard platform; (c) Interpretation of Radargram No. 54 (Profile 043), 220 kV switchyard platform; (d) Interpretation of Radargram No. 60 (Profile 060), stop-log storage area, along the line of observed ground disturbance [Author's material]

Profile 034 (switchyard platform, 88 m; ~6 m at v ≈ 0.085 m/ns; Fig. 9a). Drilling on the platform is prohibited because of the high-voltage equipment, so GPR is the only subsurface method available here. The near-surface reflector package (to ~15-20 ns) is thin and irregular. This is consistent with a graded, compacted pavement and fill rather than a monolithic slab. The upper ~2 m contain only minor local features. The deeper part of the section shows faint, broad hyperbolic arcs and, below ~4 m, sets of dipping events in the lower corners. These events are of the same type as on Profiles 040 and 043 and are attributed to above-ground structures. Field observations indicate fill to 1.5-2.0 m depth over crushed-stone soil and local objects at 0.5-2.0 m depth. No anomalous zones of loosening or settlement were found. A zone of elevated moisture at 0.2-1.5 m depth appears on most switchyard records. It is attributed to rainfall infiltration a few days before the survey. Boreholes Nos. 8 and 9, drilled around the platform in 2010, and borehole No. 12 at its southern boundary found no water-saturated soils.

Profile 040 (switchyard platform, ~104 m; ~6 m; Fig. 9b) contains five large hyperbolae with apexes near Pk 18, 32, 46, 67 and 87 m at ~35-55 ns. Their limbs remain visible 10-15 m from the apex. This corresponds to an apparent velocity of ~0.2 m/ns, more than twice the velocity adopted for the switchyard subgrade (0.085 m/ns). A buried point scatterer cannot produce such a velocity, so the signal must have travelled at least partly through air. The hyperbolae are therefore attributed to above-ground switchyard structures, such as portals and equipment supports, beside the survey line. They are not a buried pile array of the type documented in [23]. This interpretation should be checked against the as-built layout of the switchyard. A small, compact reflection at Pk ~86 m and ~40 ns (~1.4 m) is consistent with the local buried objects observed at 0.5-2.0 m depth.

Profile 043 (switchyard platform, ~36 m; ~6 m; Fig. 9c) is dominated by two broad hyperbolae with apexes near Pk 3 m and 32 m at ~80 ns. Their limbs intersect near Pk 17-18 m at ~130-140 ns and form a V-shaped pattern. Weaker hyperbolae of the same type occur at ~30-60 ns. The curvature of the limbs corresponds to an apparent velocity of ~0.3 m/ns, the velocity in air. The same pattern

https://doi.org/10.51488/1680-080X/2026.3-04

appears on the adjacent Profile 042. It is therefore attributed to reflections from above-ground objects, not to a buried object at Pk 17-18 m.

Radargram No. 60 (Profile 060, stop-log storage area, 105 m; ~0-97 ns, ~6.3 m at v ≈ 0.14-0.15 m/ns; Fig. 9d) was recorded along the line of ground disturbance. Four anomalous zones of loosening are outlined on the original record. Zone 1 (Pk ~10-25 m, from the surface to ~2.7 m) is a downward-tapering, funnel-shaped disruption. It is consistent with a local near-surface subsidence feature. Zones 2 and 3 (Pk ~35-50 m and ~54.5-70.5 m, from ~3.5 m to the base of the record at ~6.3 m) are the largest anomalies of the survey. Each shows dense, chaotic, high-amplitude scattering over ~15-16 m. This indicates intense loosening of the ground, and voids cannot be excluded. Both zones reach the base of the record, so their lower boundaries are not resolved. At the western edge of Zone 3 (Pk ~55 m), a narrow vertical band of high-amplitude reflections extends from the surface to the base of the record. It may correspond to the support post or to the vertical cavity observed at the site. Zone 4 (Pk ~96-104 m, ~1.2-2.6 m) is smaller. Surface water from rainfall and snowmelt enters a vertical cavity near a support post. The cavity formed at the contact between the reinforced-concrete and soil cover of the site. Extending the reinforced-concrete cover to the boundary of the storage area and installing a drainage system are recommended.

Table 6 - Diagnostic signatures of the switchyard and stop-log storage records (Profiles 034, 040, 043, 060) [Author's material]

Profile (Fig.)	Signature	Geometry	Interpreted origin	Recommended action
034 (Fig. 9 (a))	Minor local features in the upper ~2 m; faint broad arcs and dipping events below ~4 m	Deeper events of the same type as on Profiles 040 and 043	Graded, compacted fill without loosening; deeper events from above-ground structures	Correlate with as-built switchyard drawings
040 (Fig. 9 (b))	Five large hyperbolae, apexes at ~35-55 ns; compact reflection at Pk ~86 m (~1.4 m)	Wide limbs; apparent velocity 0.20 m/ns	Above-ground structures beside the line; local buried object at Pk ~86 m	Confirm against the as-built layout
043 (Fig. 9 (c))	Two broad hyperbolae with intersecting limbs (V pattern)	Apparent velocity ≈0.3 m/ns; repeated on Profile 042	Reflections from above-ground objects	Exclude from the subsurface interpretation
060 (Fig. 9 (d))	Four zones: funnel-shaped subsidence, two chaotic scattering zones, smaller shallow zone	Irregular, high-amplitude; up to ~16 m wide; ~3.5 m to the base of the record (~6.3 m)	Intense loosening of the ground; voids not excluded	Highest priority: test pits or probing; drainage and cover extension

These four records show how the geometry of an anomaly indicates its origin (Table 6). Compact reflections in the upper ~2 m (Profile 040, Pk ~86 m) indicate local buried objects. Broad hyperbolae with apparent velocities of ~0.2-0.3 m/ns (Profiles 034, 040 and 043) are too wide for the ground velocity. They are reflections from above-ground structures and must be excluded from the subsurface interpretation. Chaotic, high-amplitude scattering over 15 m or more (Radargram No. 60) indicates intense loosening of the ground. Comparing the apparent velocity of each hyperbola with the velocity of the medium is therefore a simple safeguard. It prevents reflections from the dense above-ground infrastructure of a hydropower site from being misinterpreted as subsurface features.

https://doi.org/10.51488/1680-080X/2026.3-04

4 CONCLUSIONS

The GPR survey of the Kapchagay HPP covered six structural elements with 62 records. The condition of each element was assessed by four criteria: continuity of the reinforced-concrete slabs, compaction of the underlying soil, presence of possible voids, and origin of the recorded anomalies. On this basis, the following conclusions can be drawn.

1. The reinforced-concrete slope protection of the river-bed dam and the tailrace channel lining show continuous slab reflectors. No major discontinuities or large voids beneath the slabs were found. Because the slabs are only 0.20-0.30 m thick, thin delaminations cannot be excluded at the frequencies used. The tailrace channel lining shows local differential settlement of the slabs over about 35 m (Profile 003).
2. Loosened soil occurs beneath the tailrace channel lining at 0.8-2.0 m depth and beneath the ravine dam slope protection at 0.9-1.5 m depth.
3. Zones of reduced compaction extend to 1.1-1.9 m depth. They occupy about 36% of the longitudinal and 32% of the transverse profile length. The zones are distributed across the platform but do not form a continuous layer. No loosening associated with concentrated seepage was found.
4. The most significant anomalies occur in the stop-log storage area (Profile 060). A near-surface funnel-shaped subsidence feature extends to about 2.7 m depth. Two zones of chaotic, high-amplitude scattering, 15-16 m wide, extend from about 3.5 m to the base of the record. They indicate intense loosening of the ground, and voids cannot be excluded. The loosening is related to surface water entering a vertical cavity near a support post.
5. Comparing the apparent velocity of diffraction hyperbolae with the velocity of the ground separates buried objects from reflections from above-ground structures. The large hyperbolae on the switchyard profiles (040 and 043) have apparent velocities of 0.2-0.3 m/ns and are caused by above-ground structures. Compact reflections in the upper 2 m indicate local buried objects.
6. The investigated structures show no evidence of widespread subsurface deterioration. The stop-log storage area should be investigated first by test pits or probing. To stop further loosening there, the reinforced-concrete cover should be extended to the boundary of the storage area and a drainage system installed. Repeated GPR surveys along the same profiles are needed to establish whether the settlement of the tailrace channel lining is stable or progressive.

REFERENCES

1. **Krüger, F., Kulikova, G., Landgraf, A.** (2018). Magnitudes for the historical 1885 (Belovodskoe), the 1887 (Verny) and the 1889 (Chilik) earthquakes in Central Asia determined from magnetogram recordings. Geophys. J. Int. 215(3), 1824–1840. https://doi.org/10.1093/gji/ggy377
2. **Landgraf, A., Dzhumabaeva, A., Abdrakhmatov, K.E., Strecker, M.R., Macaulay, E.A., Arrowsmith, J.R., Sudhaus, H., Preusser, F., Rugel, G., Merchel, S.** (2016). Repeated large-magnitude earthquakes in a tectonically active, low-strain continental interior: The northern Tien Shan, Kyrgyzstan. J. Geophys. Res. Solid Earth 121(5), 3888–3910. https://doi.org/10.1002/2015JB012714
3. **Arrowsmith, J.R., Crosby, C.J., Korzhenkov, A.M., Mamyrov, E., Povolotskaya, I., Guralnik, B., Landgraf, A.** (2017). Surface rupture of the 1911 Kebin (Chon-Kemin) earthquake, Northern Tien Shan, Kyrgyzstan. Geol. Soc. Lond. Spec. Publ. 432(1), 233–253. https://doi.org/10.1144/SP432.10
4. **Moldamuratov, Zh., Kareken, G., Ilyassova, K., Abyieva, G., Shanshabayev, N., Lapin, V., Tasmaganbetova, A., Tukhtamisheva, A.** (2026). Seismic response and frequency-dependent amplification of the Kapchagay earthfill dam from instrumental bedrock-to-crest earthquake records. ES Materials and Manufacturing, 10.30919/mm2547

https://doi.org/10.51488/1680-080X/2026.3-04

5. **Talgarbayeva, D., Vilayev, A., Dedova, T., Kuznetsova, O., Balakay, L., Merekeyev, A.** (2026). Geodynamic characterization of hydraulic structures in seismically active Almaty using lineament analysis. GeoHazards 7(1), 11. https://doi.org/10.3390/geohazards7010011
6. **Grützner, C., Walker, R.T., Abdrakhmatov, K.E., Mukambaev, A., Elliott, A.J.; Elliott, J.R.** (2017). Active tectonics around Almaty and along the Zailisky Alatau rangefront. Tectonics 36, 2192–2226. https://doi.org/10.1002/2017TC004657
7. **Rebetsky, Yu.L., Kuzikov, S.I.** (2016). Active faults of the northern Tien Shan: Tectonophysical zoning of seismic risk. Russ. Geol. Geophys. 57, 967–983. https://doi.org/10.1016/j.rgg.2016.05.004
8. **Talgarbayeva, D., Vilyaev, A., Dedova, T., Kuznetsova, O., Jangulova, G.** (2025). InSAR monitoring of dam deformations in a seismically active region of Kazakhstan for identifying precursors of failure. Front. Earth Sci. 13, 1638088. https://doi.org/10.3389/feart.2025.1638088
9. **Lee, Y.-H., Yamakawa, S., Tobita, T., Hong, H.-K., Song, H.-S., Kim, J.-J., Lee, D.-W.** (2023). Centrifugal model study of seepage and seismic behavior in a homogeneous reservoir dam with parapet. Appl. Sci. 13(10), 6347. https://doi.org/10.3390/app13106347
10. **SN RK 3.04-01-2023.** (2023). Hydraulic Structures; Committee for Construction and Housing and Utilities, Ministry of Industry and Construction of the Republic of Kazakhstan: Astana, Kazakhstan, (In Russian)
11. **Bigman, D.P., Day, D.J.** (2022). Ground penetrating radar inspection of a large concrete spillway: A case-study using SFCW GPR at a hydroelectric dam. Case Stud. Constr. Mater. 16, e00975. https://doi.org/10.1016/j.cscm.2022.e00975
12. **Pueyo Anchuela, Ó., Frongia, P., Di Gregorio, F., Casas Sainz, A.M., Pocoví Juan, A.** (2018). Internal characterization of embankment dams using ground penetrating radar (GPR) and thermographic analysis: A case study of the Medau Zirimilis Dam (Sardinia, Italy). Eng. Geol. 237, 129–139. https://doi.org/10.1016/j.enggeo.2018.02.015
13. **Gerea, A.G., Mihai, A.E.** (2024). Exploring the ground-penetrating radar technique's effectiveness in diagnosing hydropower dam crest conditions: Insights from Gura Apelor and Herculane dams, Romania. Appl. Sci. 14, 7212. https://doi.org/10.3390/app14167212
14. **Moldamuratov, Zh.N., Ilyassova, K.I., Vatin, N.I., Kareken, G.T., Shanshabayev, N.A., Orazov, S.E., Yessenkeldin, A.M.** (2026). Non-destructive ground penetrating radar inspection of hydraulic structures using the OKO-3 georadar for detection of hidden defects and assessment of technical condition. Bulletin of the Kazakh Leading Academy of Architecture and Civil Engineering (1). https://doi.org/10.51488/1680-080X/2026.1-28
15. **Moldamuratov, Zh.N., Bryantsev, A.A., Kareken, G.T., Shanshabayev, N.A., Tukhtamisheva, A.Z., Seitkazinov, O.D.** (2025). Multifactor assessment of hydraulic structures in seismically active zones: A case study of the Tasotkel reservoir, Republic of Kazakhstan. Bulletin of the Kazakh Leading Academy of Architecture and Civil Engineering (2). https://doi.org/10.51488/1680-080X/2025.2-08
16. **Ilyassova, K.I., Vatin, N.I., Tashmukhanbetova, I.B., Moldamuratov, Zh.N.** (2025). Analysis of degradation mechanisms and justification of repair technologies for concrete hydraulic structures. Bulletin of the Kazakh Leading Academy of Architecture and Civil Engineering (3). https://doi.org/10.51488/1680-080X/2025.3-07
17. **Bessimbayev, E.T., Kyzylbayev, N.K., Shandkam, A.S., Nietbay, S.E., Begaliev, U.T**. (2026). Improving the reliability and efficiency of operation of hydraulic structures of the Astana reservoir through reconstruction and modernization. Bulletin of the Kazakh Leading Academy of Architecture and Civil Engineering (1). https://doi.org/10.51488/1680-080X/2026.1-11
18. **Jol, H.M.** (2009). Ed. Ground Penetrating Radar: Theory and Applications; Elsevier: Amsterdam, The Netherlands.
19. **Daniels, D.J.** (2004). Ground Penetrating Radar, 2nd ed.; IEE Radar, Sonar and Navigation Series 15; The Institution of Electrical Engineers: London, UK,

20. **Neal, A.** (2004). Ground-penetrating radar and its use in sedimentology: Principles, problems and progress. Earth-Sci. Rev. 66(3–4), 261–330. https://doi.org/10.1016/j.earscirev.2004.01.004
21. **Solla, M., Lorenzo, H., Rial, F.I., Novo, A.** (2012). Ground-penetrating radar for the structural evaluation of masonry bridges: Results and interpretational tools. Constr. Build. Mater. 29, 458–465. https://doi.org/10.1016/j.conbuildmat.2011.10.001
22. **Wang, P., Hu, Z., Zhao, Y., Li, X.** (2016). Experimental study of soil compaction effects on GPR signals. J. Appl. Geophys. https://doi.org/10.1016/j.jappgeo.2016.01.019
23. **Hebsur, A.V., Muniappan, N., Rao, E.P., Venkatachalam, G.** (2013),"Application of Ground Penetrating Radar for Locating Buried Impediments to Geotechnical Exploration and Piling", International Journal of Geotechnical Engineering, DOI: 10.1179/1938636213Z.00000000047

https://doi.org/10.51488/1680-080X/2026.3-04

FUNDING

The study was carried out with the financial support of the Science Committee of the Ministry of Science and Higher Education of the Republic of Kazakhstan within the framework of research project No. AP23487624.

CONFLICT OF INTEREST

The authors declare no conflict of interest.

ARTIFICIAL INTELLIGENCE STATEMENT

During the preparation of this manuscript, the authors used artificial intelligence tools solely for language editing, grammar checking, and text improvement. All scientific content, interpretations, analyses, and conclusions remain the responsibility of the authors.

AUTHOR CONTRIBUTIONS

Kareken G.T. – Conceptualization, Methodology, Investigation, Formal Analysis, Writing - Original Draft.
Moldamuratov Zh.N. – Supervision, Validation, Review & Editing.
Vatin N.I. – Supervision, Validation, Review & Editing.
Shanshabayev N.A. - Formal Analysis, Review & Editing.
Bryantsev A.A. - Formal Analysis, Review & Editing.
Orazov S. - Formal Analysis, Review & Editing.

INFORMATION ABOUT THE AUTHORS

• Kareken Gulfairuz Talgatkyzy
• PhD student
• International Educational Corporation
• 050043, Almaty, Kazakhstan
• E-mail address: gulfairuz_1997@mail.ru
• ORCID ID: https://orcid.org/0000-0002-9459-3980

• Moldamuratov Zhangazy Nurzhanovich
• PhD, professor
• International Educational Corporation
• 050043, Almaty, Kazakhstan
• E-mail address: zhanga_m_n@mail.ru
• ORCID ID: https://orcid.org/0000-0002-4573-1179

• Vatin Nikolai Ivanovich
• PhD, professor
• Peter the Great St. Petersburg Polytechnic University (SPbPU)
• 195251, St. Petersburg, Russia
• E-mail address: vatin_ni@spbstu.ru

https://doi.org/10.51488/1680-080X/2026.3-04

• ORCID ID: https://orcid.org/0000-0002-1196-8004

• N.A. Shanshabayev
• PhD
• LLP «StroyTechExpertiza»
• Taraz, Kazakhstan
• E-mail address: nucho91@mail.ru
• ORCID ID: https://orcid.org/0000-0003-4930-0488

• A.A. Bryantsev
• PhD
• LLP «RAS Engineering Research Institute»
• Almaty, Kazakhstan
• E-mail address: a.briantcev@kazgasa.kz
• ORCID ID: https://orcid.org/0000-0002-6932-8202

• S.Ye.Orazov
• PhD student
• International Educational Corporation
• 050043, Almaty, Kazakhstan
• E-mail address: sa.orazov@kazgasa.kz
• ORCID ID: https://orcid.org/0009-0001-8764-5869

Received: 15 July 2026
Revised: 05 August 2026
Accepted: 20 September 2026

https://doi.org/10.51488/1680-080X/2026.3-04